Introducing fluorine-18 fluoromisonidazole positron emission tomography for the localisation and quantification of pig liver hypoxia

M. Piert[1], H.-J. Machulla[2], G. Becker[2], A. Stahlschmidt[2], M. Patt[2], P. Aldinger[1], P.D. Dißmann[1], H. Fischer[1], R. Bares[2], H.D. Becker[1], W. Lauchart[1]

[1] Department of General Surgery, University of Tübingen, Germany
[2] Department of Nuclear Medicine with Radiopharmacy Section, University of Tübingen, Germany

Received 27 July and in revised form 28 September 1998

Abstract. Fluorine-18 labelled fluoromisonidazole ([^{18}F]FMISO) has been shown to accumulate in hypoxic tissue in inverse proportion to tissue oxygenation. In order to evaluate the potential of [^{18}F]FMISO as a possible positron emission tomography (PET) tracer for imaging of liver tissue hypoxia, we measured the [^{18}F]FMISO uptake in 13 domestic pigs using dynamic PET scanning. Hypoxia was induced by segmental arterial hepatic occlusion. During the experimental procedure the fractional concentration of inspired oxygen (FiO_2) was set to 0.67 in group A (n=6) and to 0.21 in group B (n=7) animals. Before and after arterial occlusion, the partial pressure of O_2 in tissue (TPO_2) and the arterial blood flow were determined in normal flow and flow-impaired liver segments. Standardised uptake values [SUV=kBq tissue (in g) / body weight (in kg) × injected dose (in kBq)] for [^{18}F]FMISO were calculated from PET images obtained 3 hours after injection of about 10 MBq/kg body weight [^{18}F]FMISO. Immediately before PET scanning, the mean arterial blood flow was significantly decreased in arterially occluded segments [group A: 0.41 (0.32–0.52); group B: 0.24 (0.16–0.33) ml min^{-1} g^{-1}] compared with normal flow segments [group A: 1.05 (0.76–1.46); group B: 1.14 (0.83–1.57) ml min^{-1} g^{-1}; geometric mean (95% confidence limits); P<0.001 for both groups]. After PET scanning, the TPO_2 of occluded segments (group A: 5.1 (4.1–6.4); group B: 3.5 (2.6–4.9) mmHg] was significantly decreased compared with normal flow segments [group A: 26.4 (21.2–33.0); group B: 18.2 (13.3–25.1) mmHg; P<0.001 for both groups]. During the 3-h PET scan, the mean [^{18}F]FMISO SUV determined in occluded segments increased significantly to 3.84 (3.12–4.72) in group A and 5.7 (4.71–6.9) in group B, while the SUV remained unchanged in corresponding normal liver tissue [group A: 1.4 (1.14–1.71); group B: 1.31 (1.09–1.57); P<0.001 for both groups]. Regardless of ventilation conditions, a significant inverse exponential relationship was found between the TPO_2 and the [^{18}F]FMISO SUV (r^2=0.88, P<0.001). Our results suggest that because tracer delivery to hypoxic tissues was maintained by the portal circulation, the [^{18}F]FMISO accumulation in the liver was found to be directly related to the severity of tissue hypoxia. Thus, [^{18}F]FMISO PET allows in vivo quantification of pig liver hypoxia using simple SUV analysis as long as tracer delivery is not critically reduced.

Key words: Liver cell hypoxia – Nitroimidazole imaging – Fluorine-18 fluoromisonidazole – Positron emission tomography

Eur J Nucl Med (1999) 26:95–109

Introduction

A sufficient blood and oxygen supply is essential in order to maintain the liver's central metabolic functions. Microcirculatory disturbances occur in a variety of liver dysfunctions and may cause liver tissue hypoxia. Hypoxia has been associated with liver dysfunctions during endotoxaemia and haemorrhagic shock [1]. Chronic ethanol consumption causes changes in hepatic haemodynamics [2] and increases hepatic oxygen consumption, eventually leading to liver tissue hypoxia [3]. Hypoxia is also involved in the development of early alcoholic liver injury, although the precise mechanisms responsible remain unclear [4]. Furthermore, tissue hypoxia has been confirmed in primary liver tumours, with possible implications for their treatment and follow-up [5]. A number of liver transplant dysfunctions are related to impairment of the hepatic microcirculatory system, and the primary non-function of liver transplants has been associated with hypoxia-reperfusion injuries [6]. The microvasculature is a primary target during liver transplant rejection

Correspondence to: M. Piert, Abt. Allgemeine Chirurgie, University of Tübingen, Hoppe-Seyler Strasse 3, D-72076 Tübingen, Germany

[7]. Furthermore, vascular lesions followed by bile duct damage have been observed early in the rejection process [8]. Recently, a significant reduction in liver blood flow coupled with an increase in oxygen consumption was found during acute liver transplant rejection [9], suggesting that acute liver rejection might be associated with hypoxia. Therefore, imaging of ischaemia-induced hypoxia might be clinically useful in the diagnostics of liver transplant rejection.

The reduced blood flow following capillary destruction in various liver diseases has a strong effect on tissue oxygenation, but essential details of the ongoing reaction under such conditions are unknown. However, the capillary blood flow is only one determinant of tissue function. Because blood oxygen content, haemoglobin concentration (Hb), oxygen extraction, oxygen diffusion in tissue [10] and mitochondrial function [1] also determine the tissue's energy state, identification and quantification of tissue hypoxia can be expected to characterise organ viability better than blood flow alone. Tissue oxygenation reflects the balance between oxygen delivery and utilisation and any estimation of the tissue's partial pressure of oxygen (TPO_2) based on indices of delivery alone has to be considered incomplete [11].

Despite the importance of oxygen tissue levels for liver function, the difficulty of measuring tissue oxygenation in vivo limits its role in clinical decision making. Imaging hypoxic tissues has been possible with radiolabelled nitroimidazoles, which are known to undergo different intracellular metabolism depending on the oxygen availability within cells. The mechanism of nitroimidazole binding has been studied extensively [12–14] and has recently been reviewed [15]. The proposed mechanism of retention of misonidazole first involves diffusion of the lipophilic molecule across the cell membrane. The molecule undergoes a single electron reduction by nitroreductase enzymes, forming a potentially highly reactive molecule. In the presence of oxygen, the electron is donated to oxygen, forming the superoxide anion as the favoured reaction enabling the molecule to leave the cell. In oxygen-depleted but viable cells, re-oxidation of the molecule is a minor reaction resulting in a further stepwise reduction of the molecule, leading to cumulative intracellular binding of misonidazole products.

Misonidazole labelled with the positron-emitting isotope fluorine-18 fluoromisonidazole ([^{18}F]FMISO, half-life 109.7 min) allows external detection of nitroimidazole kinetics using positron emission tomography (PET). [^{18}F]FMISO and related compounds have been found to be suitable tracers for visualising hypoxic cells in tumours [16, 17] as well as in non-malignant tissues [18–20]. Oxygenation-dependent retention of [^{18}F]FMISO has been shown in myocyte preparations [21], in isolated heart perfusion studies [22] and in ischaemic myocardium in vivo [23–25]. Casciari and coworkers developed an extensive compartmental model in order to relate cellular oxygen concentration to [^{18}F]FMISO retention in tumours [26]. Misonidazole binding has been found to be increased in hypoxic murine liver tissue, indicating a potential application for [^{18}F]FMISO PET in the detection of liver hypoxia [27]. However, to date no attempts have been made to evaluate [^{18}F]FMISO as a "hypoxia" tracer for the liver since nitroimidazole and derivatives undergo a considerable hepatic metabolism [28]. Under aerobic conditions, the isolated perfused liver metabolises [^{18}F]FMISO predominantly to a β-glucuronide and three unidentified metabolites in minor concentrations, whereas under conditions of hypoxic perfusion the β-glucuronide is a metabolite of minor importance [29]. Imaging liver tissue hypoxia with [^{18}F]FMISO might be further complicated by the fact that the enhanced misonidazole binding to the normal liver occurs in part because that the liver functions at a significantly lower TPO_2 than other normally oxygenated tissues. Autoradiographic studies revealed that hydrogen-3 misonidazole binding was enhanced within hepatocytes surrounding hepatic veins, suggesting that the observed binding characteristics reflected normal regional oxygen tension variation within the liver tissue [27,30]. Similar results showing increased [^{3}H]misonidazole binding in the centrolobular zone compared with the periportal zone were obtained by Cobb et al. [31].

In previous in vivo experimental approaches in employed in the study of [^{18}F]FMISO kinetics, the amount of tracer delivered to the site of hypoxia was restricted by the reduction of blood flow inducing tissue hypoxia. Increased [^{18}F]FMISO retention by hypoxic tissues was, therefore, found to be limited to areas with a blood flow greater than 10% of normal flow ranges in brain [19] and myocardium [11]. In contrast to any other parenchymal organ, the dual blood supply of the liver allows the induction of hypoxia by arterial occlusion without critically reducing tracer delivery because tracer delivery is maintained by the portal circulation. To the best of our knowledge, in none of previous in vivo [^{18}F]FMISO biodistribution studies has the tissue's oxygen concentration actually been measured, thus confirming simultaneously the presence of tissue hypoxia and enhanced tracer retention.

The current study was undertaken to evaluate the potential of [^{18}F]FMISO to detect and quantify liver tissue hypoxia, by combining [^{18}F]FMISO PET and direct PO_2 measurements of the liver tissue. To determine liver tissue oxygen concentrations, the commercially available polarographic oxygen sensor system, Eppendorf PO_2 Histograph, was chosen because of its relative ease of application and its ability to repeatedly measure tissue PO_2 not only on the surface but also deep inside the liver parenchyma. This device has been used in human studies to measure tissue PO_2 distribution in various tumours [32, 33]. To determine the effect of the oxygenation level of the breathing air on [^{18}F]FMISO retention, two different ventilation conditions were selected: room air ventilation to maximise possible liver hypoxia and oxygen-enriched ventilation for comparison.

Materials and methods

Experimental preparations. We established an in vivo model to study regional liver hypoxia in 13 female German landrace pigs, weighing 18–33.5 kg. Before the experiments, the animals were fasted for 24 h with free access to water. The animals were premedicated with an intramuscular injection of 120 mg azaperon, 2 mg flunitrazepam, 200 mg ketamine and 1 mg atropin-sulphate. After induction of the anaesthesia using a mixture of O_2 and N_2O gases the animals were intubated and ventilated continuously by a respirator with N_2O, O_2 and 0.8%–1.0% of isoflurane (Sulla 800 V, Draeger, Germany). The tidal volume was set to 10–13 ml/kg body weight with a frequency of 10–12/min, modified according to the results of frequent arterial blood gas analyses so as to keep the PCO_2 within the normal range. Throughout the experiment body temperature was kept constant at about 36°C with a heating mat. ECG and systemic blood pressure were recorded continuously (Hewlett Packard 78354 A, Böblingen, Germany).

The abdomen was opened by a midline incision. For arterial microsphere injections and blood pressure measurements, a polyethylene catheter (2.1 mm diameter) was inserted into the left iliac artery and advanced to the descending thoracic aorta under angiographic guidance (BV25 Philips, Germany). A second arterial catheter was inserted into the right iliac artery and advanced to the abdominal aorta to collect the reference sample during microsphere injections and for continuous blood sampling during the scan using a pump system. A large iliac vein was cannulised and the inserted 3.3-mm catheter was advanced to the distal inferior vena cava for fluid substitutions. To permit bile and urine volume measurements, the common bile duct and both ureters were cannulised. A 2.1-mm catheter was inserted into a pancreatic vein and advanced to the stem of the portal vein to allow portal venous blood gas analyses (Stat 9 Profile, Nova Biomedical, Germany). The correct location of the catheter's tip was checked manually and angiographically. The liver tissue oxygen distribution was measured by direct PO_2 histography (T_1) (see below). The animals were haemodiluted to a mean arterial haemoglobin concentration of 8.4 mg/dl (group A) or 9.1 mg/dl (group B), replacing 300 ml of blood with 300 ml 6% dextran solution, and fully heparinised to avoid clotting of catheters. The arterial blood flow of abdominal organs was measured by chromium-51 labelled microspheres (see below). Then, several branches of the left or right hepatic artery were ligated to diminish the arterial blood flow to corresponding liver segments. Flow-impaired liver segments were identified visually by their change in surface appearance and marked by surface coagulation for later identification. The PO_2-histography was repeated in flow-impaired and normal flow segments (T_2). The abdomen was closed after flushing of all catheters.

Approvals. The experimental protocol was reviewed and approved by the Animal Research Committee of the Administrative District of Tübingen. The institutional guidelines for the care and use of laboratory animals were followed throughout the study.

Tissue PO_2 measurements. After calibration, the liver tissue oxygen distribution was measured directly by PO_2-histography (PO_2-Histograph Model 6650, Eppendorf, Hamburg, Germany). During the experimental procedure the fractional concentration of inspired oxygen (FiO_2) was set to 0.67 (O_2:N_2O=2:1) in group A (n=6) and to 0.21 (room air ventilation) in group B (n=7). After arterial occlusion (T_2), the liver TPO_2 was determined in normal flow and flow-impaired liver segments under oxygen-enriched and room air ventilation. Before measurements were taken, ventilation conditions were kept constant for at least 15 min and additional arterial and portal venous blood gas analyses were performed. The liver segment was gently exposed to the probe by the surgeon reducing liver movements due to ventilation. The needle electrode was inserted about 2 cm into the tissue with an angle of 10–30° and allowed to equilibrate. Then six to ten tracks were measured per segment, with the tracks averaging 20 mm in length, resulting in 120–200 single PO_2 measurements. Measurements were taken from normal and flow-impaired liver segments, forwarding the needle automatically in 1-mm steps (a rapid forward movement of 1.3 mm was followed by a backward movement of 0.3 mm to minimise compression effects caused by forward motion of the needle). The point of needle entry into the liver was marked by surface coagulation. The results were expressed as the geometric mean and 95% confidence limits of each tissue histogram. Individual TPO_2 results were then pooled into frequency histograms summarising the measurements of each group as percentages of relative frequency of the TPO_2 in mm Hg at various time points.

In additional experiments, the reproducibility of oxygen tension measurements in liver tissues was established by repeated measurement of the TPO_2. Under stable ventilation conditions (either oxygen-enriched or room air ventilation), the TPO_2 was measured twice within 30 min in normal and flow-impaired liver. We were unable to detect changes in the TPO_2 under these conditions. The variability of PO_2 measurements expressed as the coefficient of variation (COV=SD/mean ×100) was determined under various conditions and found to be 2.6 in saline solution and 2.2 in oxygen-inflated saline solution. Based on this information, negative values exceeding –2.5 mmHg were excluded, because they were likely due to blockages of the probe membrane or pressure artefacts rather than to deviations from a mean of 0 mmHg (Eppendorf, personal communication, May 1996).

Radiotracer. Fluorine-18 was produced at the cyclotron (PETtrace, General Electric, USA) by irradiating 97% oxygen-18 enriched water with 16.5 MeV protons. The preparation of the radiotracer was performed in a two-step synthesis as described previously [34, 35]. Briefly, [^{18}F]epifluorohydrin was prepared by aminopolyether-supported substitution of tosylate with potassium [^{18}F]fluoride in (*R*)-(–)-glycidyltosylate. [^{18}F]FMISO was obtained from the reaction of [^{18}F]epifluorohydrin with 2-nitroimidazole, purified by high pressure liquid chromatography (HPLC) and formulated in physiological saline. The overall time of synthesis was 60 min. Radiochemical and chemical purities were determined by HPLC analysis of the final injection solution and were higher than 99% and 97%, respectively. Specific activity was about 37 TBq/mmol (1000 Ci/mmol) at the end of bombardment. [^{18}F]FMISO was shown to be stable for at least 6 h by repeated HPLC analyses.

Scanning procedure. Immediately before the PET scan, the arterial blood flow was again measured by microspheres injection (T_3) (see below). The PET scans were started on average 3 h after ligation of arterial branches of the hepatic artery using a high-resolution PET scanner (Advance, General Electric, USA). Under optimal laboratory conditions (National Electronics Manufactures Association performance standard), the PET scanner reaches a spatial resolution of approximately 5 mm full-width at half-maximum (FWHM) at the centre of the field of view [36], while the resolution is considerably lower during dynamic image acquisition (about 8–10 mm FWHM).

The animals were scanned in the supine position, ventilated with either oxygen-enriched (group A, n=6, body weight 26.9±3.2 kg) or room air (group B, n=7, body weight

26.4±5.6 kg). Anaesthesia was maintained by repeated intravenous injections of ketamine and diazepam as needed. After positioning of the liver into the scanner's 15.2-cm field of view, a 20-min measured transmission scan was acquired using a pair of rotating germainim-68 pin sources (half-life 270.8 days). About 10 MBq/kg body weight [^{18}F]FMISO was injected into a peripheral ear vein within 10 s. Simultaneously, a dynamic emission sequence of 34 PET scans was started for 180 min according to the following protocol: 12×10 s, 6×30 s, 5×5 min, 3×10 min, 8×15 min (T_4). Arterial and portal venous blood samples were taken manually into heparinised syringes as rapidly as possible during the first 2 min following tracer injection and then at progressively longer intervals according to the imaging sequence. In addition, blood of the abdominal aorta was withdrawn continuously for about 30 min at a rate of 16 ml/min by a calibrated infusion pump system (IMED Corporation Gemini PC-1, San Diego, Calif., USA). Using an initial 2-s counting interval, whole blood radioactivity was measured continuously by a calibrated NaI detector system (Blood Sampler FRQ, General Electric, USA). The blood leaving the detector system was reinfused into the inferior vena cava.

Immediately after the end of the PET scan, the abdomen was reopened and PO_2 histography was repeated in the same liver segments where measurements had been taken during the operation (T_5). Then, the animals were sacrificed. The liver was rapidly excised and placed into a plastic container to perform an additional 10-min static PET scan followed by a 10-min transmission scan to identify the TPO_2-measured liver segments in the dynamic image sequence. TPO_2-measured liver segments (identified by surface coagulation) were marked by solid metal screws, which were clearly seen on transmission images. In the meantime, tissue samples from several organs were taken for radioactivity counting. After the end of the static organ PET scan (about 30 min after death), the liver was harvested (T_6).

Histology. Immediately after sacrifice, liver tissue samples of about 1 g were collected from TPO_2-measured flow-impaired and normal flow regions and fixed with formalin after removal of excessive blood. After decay of the radioactivity, the liver tissue was cut into 10-µm sections. The samples were stained with haematoxylin-eosin. To assess liver tissue reactions to the arterial occlusion, a histological score developed to quantify hypoxia-related liver tissue changes was applied, yielding a score index characterising the severity of hypoxia [37]. The following light microscopic findings were evaluated: liver surface reactions, portal cell infiltration, single cell necroses and centrolobular necroses, interstitial oedema, intracellular oedema, fatty cell degeneration, hyperaemia, bleeding, subcapsular necrosis, focal liver cell necrosis and hepatocytic mass necrosis. The slices were observed by independent observers unaware of the experimental procedure.

Microsphere measurements and tissue sampling. The arterial reference method was used for microsphere flow measurements [38]. 2.0±0.2 MBq microspheres (diameter: 15.5±0.1 µm) labelled with either ^{51}Cr or cerium-141 (DuPont, USA) were injected into the thoracic aorta within 10 s. Arterial reference samples were withdrawn over 90 s at a rate of 16 ml/min from the iliac artery starting 5 s before tracer injection (Microlab M, Hamilton, Germany). The half-lives of ^{51}Cr and ^{141}Ce are 27.7 and 32.5 days, respectively.

After sacrifice, the liver was harvested and multiple tissue samples of approximately 0.3–0.5 g were dissected from all parts of the liver according to individually drawn "liver maps". To allow comparisons with PET measurements of individual animals, 12 regions of the liver were defined according to their location. Eight regions were defined in the right and four in the left lobe; half of them were dorsal and half ventral, resulting in four ventral right, four dorsal right, two ventral left and two dorsal left regions. Those tissue samples where PO_2 measurements had been taken and metal screws had been inserted for static PET scanning were identified separately. In addition, tissue samples from lung, spleen, stomach, pancreas, muscle, heart, small and large intestine were obtained for radioactivity counting of ^{18}F activity by a calibrated two channel scintillation counter (Wizard 1480, Wallac, Finland). After complete ^{18}F decay, ^{51}Cr and ^{141}Ce activity from microspheres was counted. Corrections were made for spillover and decay. Significant microsphere shunting was not observed. In order to describe the spatial variability of the regional arterial blood flow to the liver, the relative dispersion was calculated according to the method of Zwissler et al. [39]. Tissue activities from administered [^{18}F]FMISO were calculated as standardised uptake value [SUV=kBq tissue (in g)/body weight (in kg)× injected dose (in kBq)].

Image processing. PET data were corrected for scatter, deadtime and attenuation using a Hanning 0.35-mm filter. The radioactivity measured in tissue and blood was corrected for decay and adjusted for time shift. To ensure correct identification of anatomical structures, the images were reconstructed axially and coronally (slice thickness 4.3 mm). Six standardised circular ROIs (size: 2.0 cm^2) were drawn in normal flow and flow-impaired segments of TPO_2-measured liver regions. The images of the second static PET scan were used to identify these anatomical regions in the dynamic PET image sequence. To minimise possible errors due to misidentification, the mean results of three normal and three flow-impaired ROIs were taken for further calculations. In addition, flow impairment was verified in axially and coronally summed blood pool images of the first 5 min (summation of image set 1–15). The SUV was calculated in each ROI from the last image of the dynamic sequence (165–180 min).

Statistics. Because variances were not equally distributed between groups, all statistical tests were performed after logarithmic transformation of the data. To evaluate group differences, data were subjected to a two-way analysis of variance taking into account interactions between groups (group A and B) and type of tissue (normoxic and hypoxic) and, when appropriate, repeated measurements as well, followed by post-hoc *t* tests. Linear and non-linear regressions were calculated by the least-squares method. Unless otherwise stated, results are expressed as geometric mean values of parameters with their respective 95% confidence limits. Probabilities <0.05 were taken to indicate statistically significant differences. Statistical tests were performed with the JMP statistical software package.

Results

Blood gas analyses, haemodynamic data and TPO_2 results

The effects of haemodilution, microsphere injections and arterial occlusion on the liver's oxygen tension were investigated in five experiments, three under group A and two under group B conditions. The mean TPO_2 was determined before haemodilution [group A: 23.5 (20.8–26.5); group B: 22.2 (19.5–25.3) mmHg), after

Table 1. Haemodynamic and laboratory results of groups A and B at different time points during the experiment

Group	Time point[a]	Arterial haemoglobin (mg/dl)	Arterial PO_2 (mmHg)	Arterial SO_2 (%)	Arterial O_2 content (ml ml^{-1})	Portal venous haemoglobin (mg/dl)	Portal venous PO_2 (mmHg)	Portal venous SO_2 (%)	Portal venous O_2 content (ml ml^{-1})	Heart rate (min^{-1})	MAP (mmHg)
A	T_1	8.4 (7.6–9.3)	288 (251–330)	99.1 (97.5–101)	0.120 (0.108–0.133)	9.0 (8.2–9.8)	61.9 (54.7–70.1)	92.2 (86.0–98.8)	0.112 (0.099–0.128)	121 (110–133)	81.4 (73.5–90.2)
	T_2	9.0 (8.1–9.7)	260 (227–298)	99.2 (97.6–101)	0.128 (0.115–0.142)	9.1 (8.3–10.0)	61.4 (54.2–69.5)	85.8 (80.6–91.3)	0.107 (0.095–0.120)	115 (103–128)	79.8 (71.1–89.7)
	T_3	8.7 (7.8–9.7)	280 (244–321)	99.1 (97.5–101)	0.130 (0.116–0.146)	8.5 (7.7–9.3)	60.4 (53.4–68.4)	87.7 (82.4–93.4)	0.102 (0.091–0.114)	112 (103–122)	78.7 (71.8–86.4)
	T_4	8.7 (7.8–9.6)	275 (240–315)	99.0 (97.4–101)	0.124 (0.112–0.138)	8.7 (7.9–9.5)	64.8 (57.2–73.3)	87.7 (82.4–93.4)	0.104 (0.093–0.117)	123 (113–133)	71.9 (65.7–78.8)
	T_5	8.5 (7.7–9.4)	286 (249–328)	98.6 (97.0–100)	0.124 (0.111–0.137)	8.6 (7.9–9.4)	68.1 (60.2–77.2)	87.6 (82.2–93.2)	0.103 (0.092–0.116)	130 (115–148)	75.1 (65.6–86.1)
B	T_1	9.1 (7.5–11.0)	99.4 (77.0–128)	96.0 (93.1–99.0)	0.120 (0.099–0.146)	10.0 (8.4–11.8)	61.5 (48.7–77.5)	83.4 (74.2–93.8)	0.113 (0.091–0.140)	128 (118–139)	75.0 (68.9–81.6)
	T_2	9.9 (8.8–11.2)	85.0 (72.8–99.3)	93.5 (91.5–95.5)	0.129 (0.113–0.148)	9.5 (8.6–10.5)	50.3 (43.7–58.0)	73.9 (68.2–80.1)	0.099 (0.086–0.115)	127 (117–137)	79.7 (73.2–86.7)
	T_3	9.6 (8.8–10.6)	83.3 (73.4–94.5)	95.8 (94.4–97.2)	0.118 (0.106–0.131)	9.6 (8.8–10.4)	41.0 (36.5–45.9)	76.0 (71.7–80.5)	0.092 (0.081–0.103)	123 (114–133)	76.8 (70.6–83.6)
	T_4	8.8 (8.0–9.7)	75.7 (66.7–85.9)	94.8 (93.4–96.2)	0.114 (0.104–0.126)	9.1 (8.4–9.9)	40.2 (35.8–45.1)	73.7 (69.5–78.0)	0.091 (0.082–0.101)	124 (115–135)	75.6 (69.5–82.3)
	T_5	9.1 (8.3–10.1)	72.9 (64.3–82.8)	94.4 (93.0–95.8)	0.118 (0.107–0.130)	8.9 (8.2–9.6)	39.3 (35.1–44.1)	73.3 (69.1–77.6)	0.091 (0.082–0.101)	124 (114–135)	72.3 (65.9–79.3)

Results are expressed as geometric mean and 95% confidence limits (in parentheses)

[a] T_1, before arterial occlusion; T_2, after arterial occlusion; T_3, during blood flow measurements; T_4, during PET scanning; T_5, immediately after the end of the PET scan

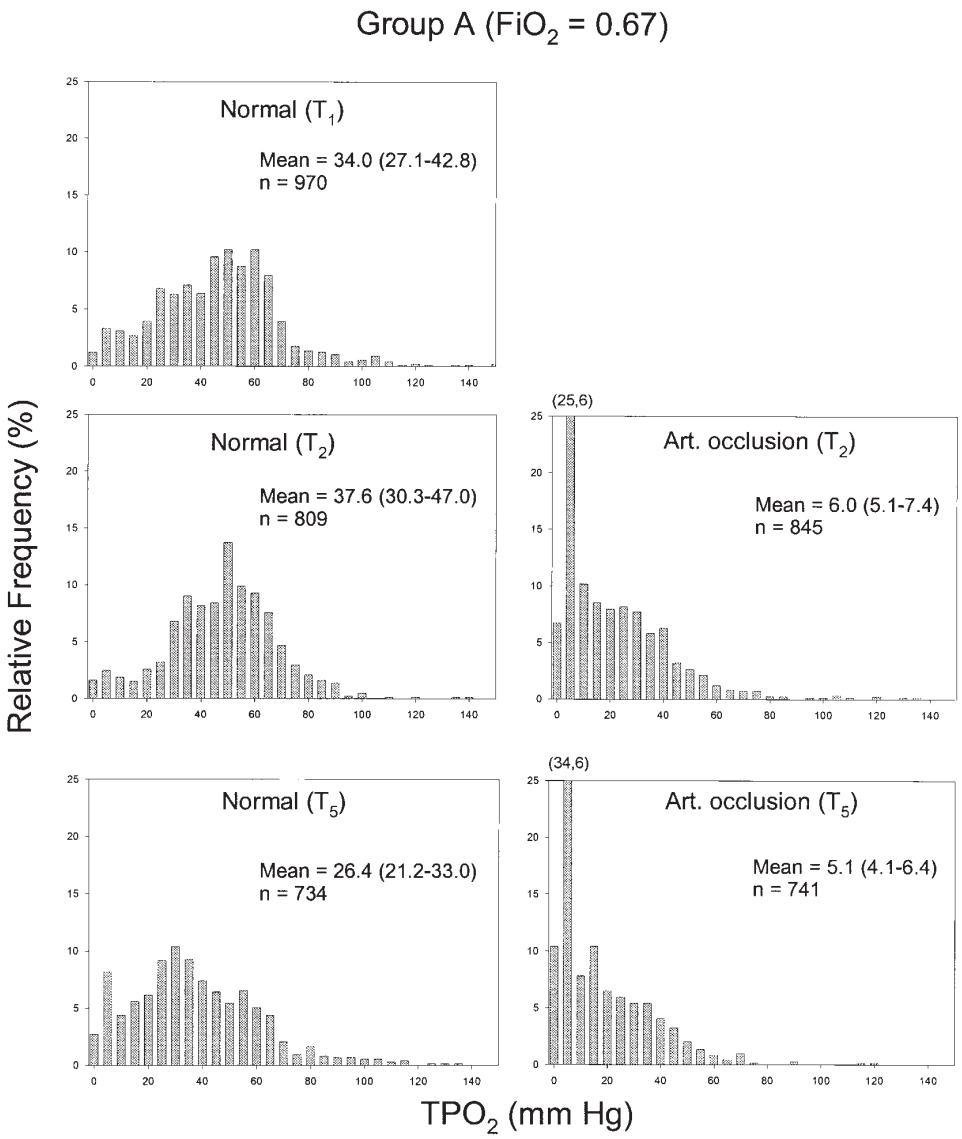

Fig. 1. Histograms of relative frequency (in%) of TPO_2 measurements (in mmHg) made with a polarographic oxygen electrode (PO_2 Histograph, Eppendorf) in normal and arterially occluded liver segments under oxygen-enriched (**a**, group A: FiO_2=0.67) and room air (**b**, group B: FiO_2=0.21) ventilation. The step size for frequency counting was 5 mmHg. Measurements were taken before (T_1) and after (T_2) arterial occlusion as well as after PET scanning (T_5). The total number of measurements (n) and the geometric mean with the upper and lower 95% confidence limits of the pooled data are shown. Numbers in parentheses above the boxes indicate values greater than 25% for the column in question

haemodilution [group A: 27.8 (25.6–30.3); group B: 20.1 (17.5–23.0) mmHg], after microsphere injection [group A: 24.4 (22.0–27.0); group B: 20.9 (18.3–23.9) mmHg] and in the presence of contralateral arterial occlusion (group A: 24.8 (22.2–27.9); group B: 26.5 (23.9–29.3) mmHg] (figures indicate geometric mean and 95% confidence limits). Since we were unable to observe significant changes in liver tissue oxygenation due to haemodilution, microsphere injection or arterial occlusion in normal flow segments, these additional measurements were omitted from the remainder of the study to shorten the experimental procedure.

Due to differing ventilation conditions, the mean oxygen saturation (SO_2) and PO_2 of the arterial and portal venous blood were significantly higher in group A than in group B (P<0.001) at all time points (T_1–T_5, see Table 1). No significant differences between groups A and B were observed with respect to body weight, haemoglobin concentration, heart rate or mean arterial blood pressure at any of the time points.

The pooled results of the TPO_2 measurements in normal and flow-impaired liver are given in Fig. 1 and 1B. The box plots show the relative frequency of oxygen partial pressures obtained at different time points (T_1, T_2 and T_5). Due to the differences in the oxygen content of the arterial and portal venous blood, the appearance of TPO_2 profiles varied considerably between groups. Under oxygen-enriched ventilation conditions (group A), the range of observed TPO_2 values tended towards higher PO_2 values and was, overall, significantly higher compared with the room air ventilation group B (P<0.05). In both groups, during the operation (T_2) as well as after PET (T_5), the mean TPO_2 measured in flow-impaired liver was significantly lower than in normal flow liver regions (P<0.001). At T_5, the TPO_2 of occluded segments was 5.1 (4.1–6.4) mmHg in group A and 3.5 (2.6–4.9) mmHg in group B, while the TPO_2 of normal flow segments was 26.4 (21.2–33.0) mmHg in group A and 18.2 (13.3–25.1) mmHg in group B (P<0.001 for both groups). The reduction of the mean TPO_2 in flow-

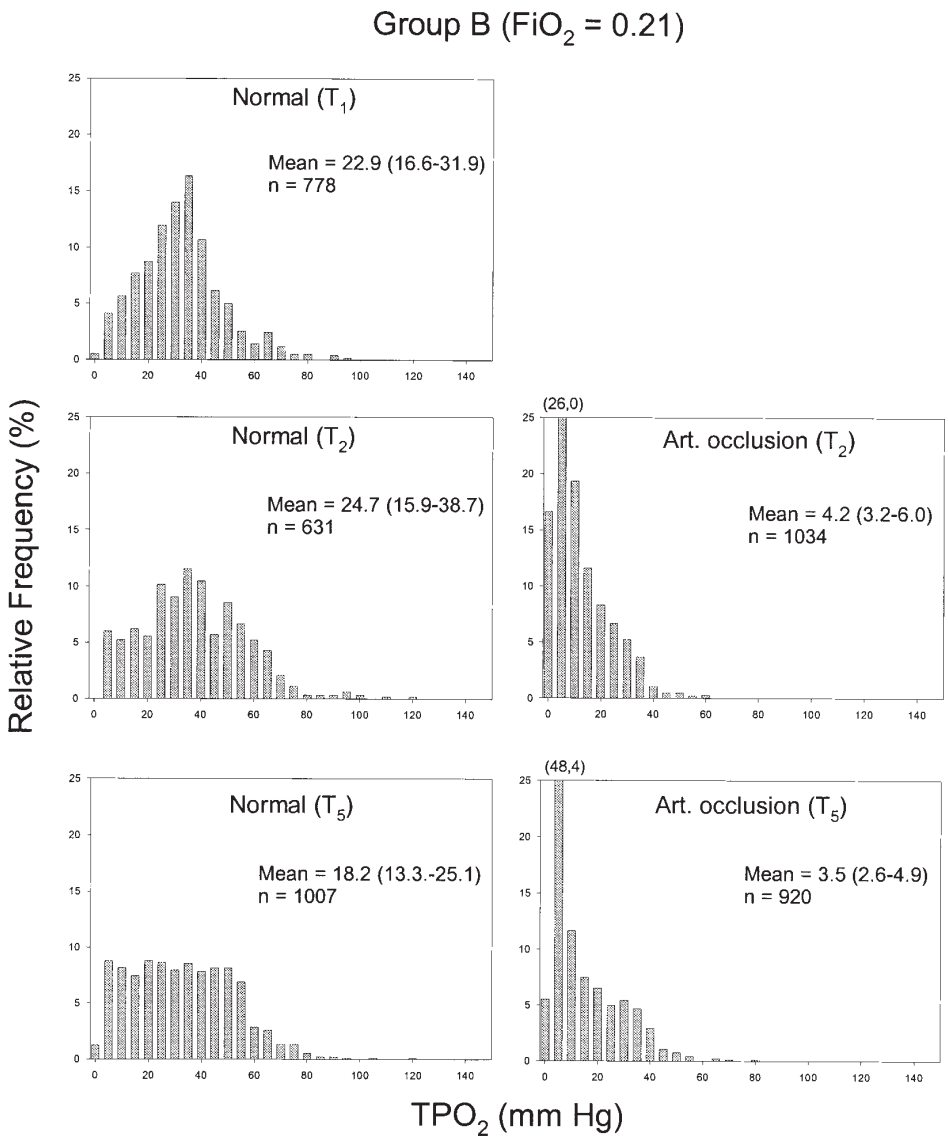

Fig. 1B

impaired liver segments was the result of a distinct shift of the distribution curve to the left. Over time, a slight decline in the mean TPO_2 of flow-impaired and normal liver was noticed. This decline failed to reach statistical significance in normal liver tissue or flow-impaired segments of either group.

PET results

Figure 2 shows transaxial reconstructions of summed [^{18}F]FMISO PET images of a group B experiment. While the right liver lobe displays intense activity in early images due to normal liver perfusion, the left liver lobe shows low tracer uptake due to arterial occlusion of the left branch of the hepatic artery. In contrast, [^{18}F]FMISO accumulation is high in the left liver due to tracer entrapment, while [^{18}F]FMISO did not accumulate in the right liver lobe. The placement of circular ROIs in normal and hypoxic liver is shown.

[^{18}F]FMISO time-activity curves of arterial whole blood, arterial plasma, portal venous and central venous blood were generated for each experiment. Plasma activity was found to be consistently 2%–5% higher than whole blood activity, with very small time-dependent individual or interindividual variations. After injection, [^{18}F]FMISO rapidly redistributed followed by a slow clearance phase. Using the arterial plasma time-activity curves, the whole body drug clearance was calculated as $T_{1/2}$=308.4±128.1 min in group A and 335.9±149.6 min in group B experiments (arithmetic mean ±SD).

Cumulative time-activity curves of normal flow and flow-impaired liver regions of group A and B experiments as well as the arterial plasma input curves are shown in Fig. 3. After an initial activity peak due to the tracer injection, the [^{18}F]FMISO SUV in normal liver followed the decrease in blood pool activity but remained constantly elevated when compared with plasma. The graph shows that the SUV of normal flow regions was slightly higher in group B than in time-equivalent

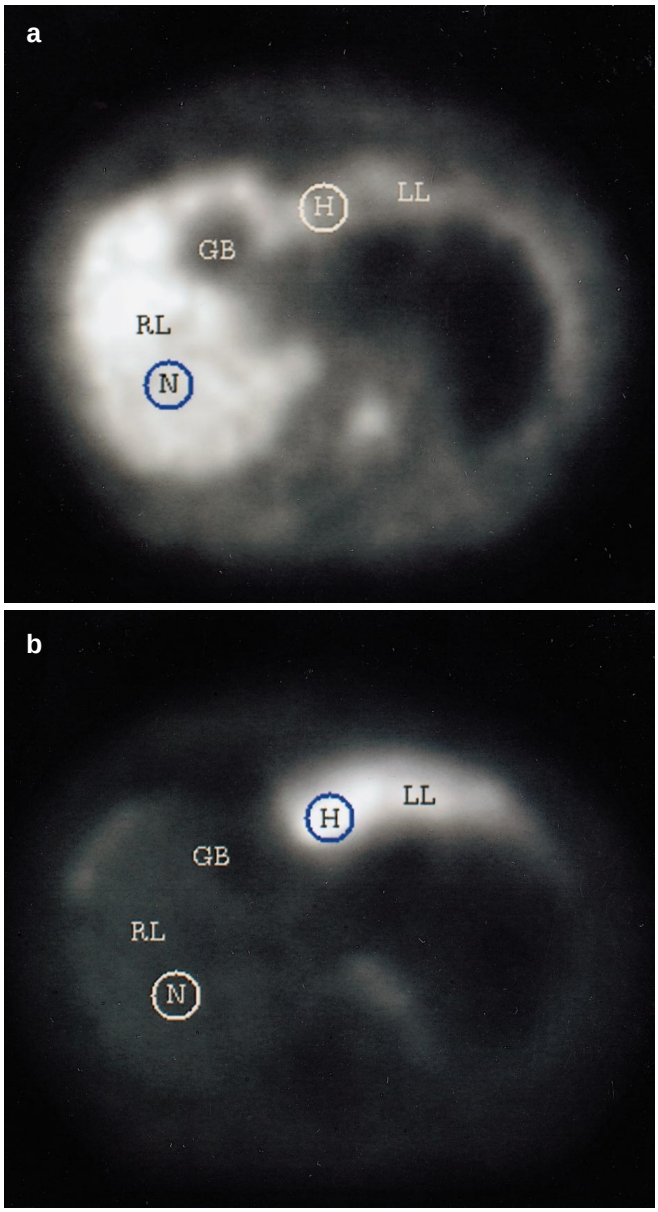

Fig. 2a, b. Transaxial PET images of the upper abdomen obtained after i.v. injection of 255 MBq of [^{18}F]FMISO in a group B animal. **a** Summation of the first 5 min of the dynamic image sequence (perfusion image), **b** summation between 165 and 180 min (accumulation image). The normally perfused right liver lobe (*RL*) shows intense activity in the early image, while the left liver lobe (*LL*) displays low tracer uptake due to arterial occlusion of the left branch of the hepatic artery. In contrast, accumulation from administered [^{18}F]FMISO is high in the left liver due to tracer entrapment, while [^{18}F]FMISO (and metabolites) did not accumulate in the well-oxygenated right liver lobe. No activity is seen in the gallbladder (*GB*). The circular ROIs indicate normal (*N*) and hypoxic (*H*) liver according to TPO_2 measurements before and after PET scanning. In **b**, the SUV was determined as 6.8 in hypoxic and as 1.6 in normoxic liver tissue

values of group A experiments, but the difference did not reach statistical significance. Time-activity curves obtained from flow-impaired liver segments were configured differently. Due to reduced arterial tracer delivery, the initial [^{18}F]FMISO tissue uptake (between 0 and 5 min) was decreased in flow-impaired compared with normal flow liver of both groups, with the smallest uptake seen in group B experiments. After 5 min, the ratio between the SUV of flow-impaired to normal flow regions constantly increased up to 2.7 in group A and 4.4 in group B experiments (measured 165–180 min after injection). Three hours after tracer injection, in both groups the SUV for [^{18}F]FMISO was highly significantly elevated in hypoxic liver [group A: 3.84 (3.12–4.72); group B: 5.7 (4.71–6.9)] compared to corresponding normal liver [group A: 1.4 (1.14–1.71); group B: 1.31 (1.09–1.57); $P<0.001$)] (see Table 3).

Tissue sampling data

The biodistribution from administered [^{18}F]FMISO and microsphere entrapment is shown in Table 2 for tissue samples from several organs. The measured [^{18}F] activity in tissue (defined as free and bound [^{18}F]FMISO and its metabolites) was calculated as the SUV to allow comparisons with PET measurements. Tissue activities were similar to plasma activities in most tissues, exceptions being kidney and liver. Since the measured activity in urine was much higher than blood activity and quite variable as well, elevated kidney activities indicated the urinary excretion of the drug. Repeated microspheres injections revealed no significant differences between the arterial blood flow during the PET scanning (T_3) compared with earlier measurements during the operation (T_1), although a slight increase in the range of the flow distribution was observed. Flow-impaired liver tissue samples could not be identified by simply comparing the results of the two arterial blood flow measurements because the arterial blood flow to the non-occluded liver could have been influenced by the experimental procedure. Arterial flow impairment due to arterial occlusion was stated for each liver tissue sample when the decrease in arterial blood flow exceeded the mean reduction to reference organs (spleen, pancreas, kidney and stomach). Using this approach, 446 of the 759 liver tissue samples investigated were identified as flow-impaired. Among these samples, 105 flow-impaired and 72 normal flow tissue samples were investigated from liver segments where TPO_2 measurements had been taken.

The distribution of the hepatic arterial blood flow was studied using repeated microsphere measurements before (T_1) and after segmental arterial occlusion (T_3). At both time points, the arterial blood flow to the normal liver was characterised by a moderate spatial variability (mean 16.8%–18.6%) while the spatial variability increased in occluded segments to 49.0%. The mean arterial blood flow to non-occluded liver remained un-

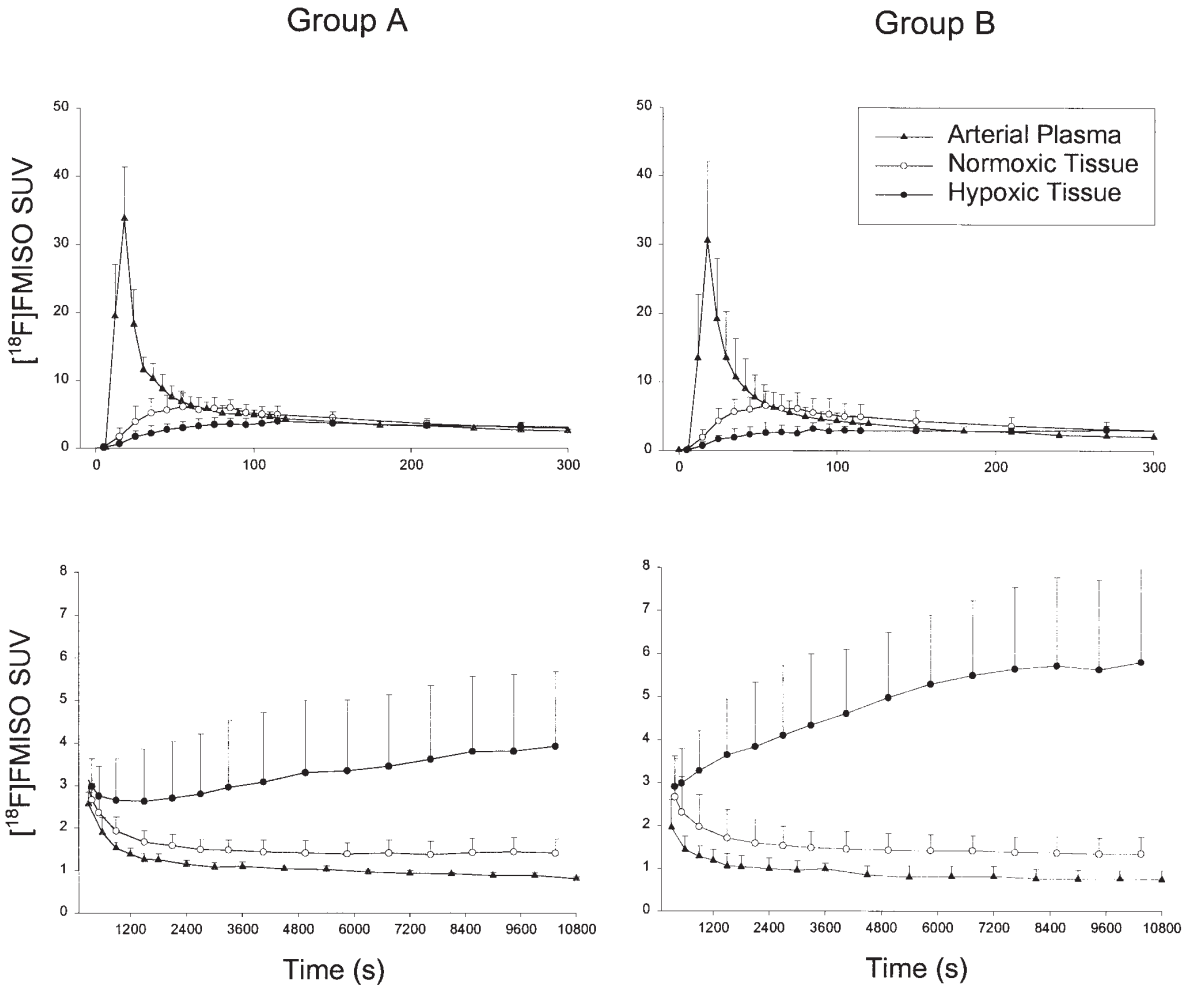

Fig. 3. Cumulative [18F]FMISO SUV time-activity curves of normal and hypoxic liver regions and cumulative arterial plasma input curves. The results are displayed as geometric mean (± standard deviation) of the SUVs for [18F]FMISO in tissue and plasma of group A (FiO_2=0.67) and group B (FiO_2=0.21) experiments

Table 2. Tissue biodistribution of administered [18F]FMISO expressed as the standard uptake value (SUV), and the arterial blood flow measured immediately before PET scanning by arterially injected microspheres (T_3)

Type of tissue	Arterial blood flow before PET (T_3) (ml min^{-1} g^{-1})	[18F]FMISO (T_6) (SUV)
Arterial plasma (180 min after inj.)	–	0.76 (0.69–0.86)
Heart	–	0.86 (0.79–0.94)
Lung	–	0.77 (0.68–0.87)
Kidney	2.36 (1.84–2.88)	1.89 (1.44–2.34)
Spleen	1.90 (1.27–2.54)	0.73 (0.64–0.82)
Muscle	0.05 (0.00–0.12)	0.78 (0.70–0.87)
Small intestine	0.56 (0.33–0.79)	1.31 (1.04–1.58)
Large intestine	0.32 (0.19–0.44)	1.08 (1.01–1.15)
Stomach	0.29 (0.14–0.44)	0.87 (0.82–0.92)
Pancreas	0.29 (0.22–0.37)	0.92 (0.84–1.01)

The tissue samples were obtained immediately after sacrifice (about 210 min after [18F]FMISO administration; T_6). The data represent the geometric mean (95% confidence limits in parentheses) of all 13 experiments. Except for kidney and intestine, tissue activities approximate those of final plasma concentrations

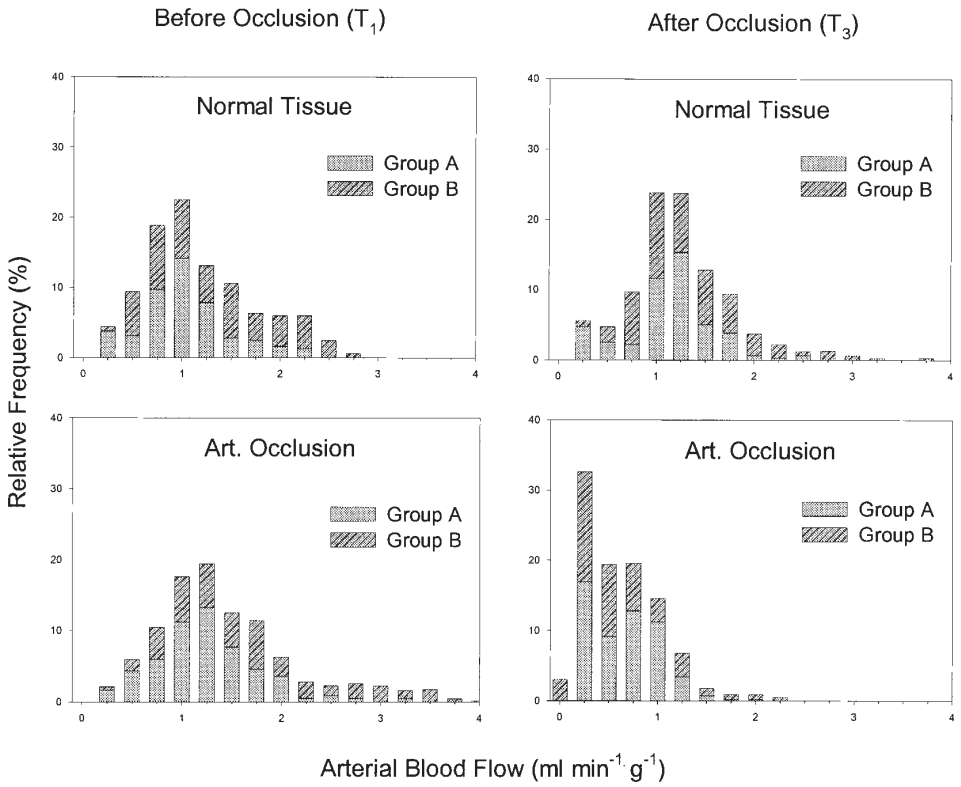

Fig. 4. Relative frequency of the arterial blood flow determined by dual arterial microsphere injections before and after segmental occlusion of a branch of the hepatic artery. Given are flow values measured in all tissue samples in normal and hypoxic liver (in ml min^{-1} g^{-1}) of group A (*grey columns*) and group B (*dark grey hatched columns*) before (T_1) and after arterial occlusion (T_3). The step size for frequency counting was 0.25 ml min^{-1} g^{-1}. Note the distinct shift of the distribution curve to the left after arterial occlusion in flow-impaired liver tissue samples

changed after segmental arterial occlusion. The regional distribution of the arterial blood flow before arterial occlusion (T_1) was assessed using the regional mapping approach. No significant differences were found between the arterial blood flow of the right or left lobe or between dorsal or ventral regions. In addition, a comparison of each individual region of both liver lobes with each other produced no significant difference between regions. Segmental occlusion resulted in a distinct shift of the flow distribution to lower values, i.e. to the left, in occluded areas, while no significant changes in arterial blood flow were seen in non-occluded segments (Fig. 4). Unexpectedly, total cessation of flow was found to occur in only 2.9% of the 446 flow-impaired liver tissue samples.

In TPO_2-measured tissue samples, the mean arterial blood flow was significantly decreased in arterially occluded segments of group A [0.41 (0.32–0.52) ml min^{-1} g^{-1}] and B [0.24 (0.16–0.33) ml min^{-1} g^{-1}] compared with normal flow segments [group A: 1.05 (0.76–1.46); group B: 1.14 (0.83–1.57) ml min^{-1} g^{-1}; $P<0.001$ for both groups].

Histology

The histological findings in normal and arterially occluded liver segments are displayed in Fig. 5. As shown in Fig. 5a, only minor light microscopic changes were found in normal liver tissue. A few biopsies depicted mild to moderate signs of intracellular and interstitial oedema. Intravascular hyperaemia and single necrotic hepatocytes were identified in some cases, especially from group B. Changes were more pronounced in arterially occluded liver biopsies of both groups. Intra- and extravascular oedema was generally observed in hypoxic liver biopsies. A pronounced subcapsular and parenchymal cell necrosis was found as well as intense intravascular hyperaemia indicating sinusoidal stasis (Fig. 5b). In both groups, the histological score findings were significantly different between flow-impaired and normal flow regions ($P<0.05$). In group A, the score was 9.7 (6.6–14.2) in normal and 22.8 (15.5–33.4) in flow-impaired liver tissue, and in group B 15.5 (10.2–23.6) and 34.5 (24.5–48.5), respectively.

Comparison of arterial blood flow, TPO_2, histological score and [^{18}F]FMISO uptake

The arterial blood flow, TPO_2 values and [^{18}F]FMISO uptake of PO_2-measured tissue (measured by PET and by direct tissue sampling) are shown in Table 3. Following to segmental arterial occlusion, the mean arterial blood flow at T_3 was decreased significantly by 65.3% in group A ($P<0.01$) and 85.4% in group B ($P<0.001$) compared with normal flow segments (group A: -15.3%; group B: -15.6%). At T_5, the TPO_2 of flow-impaired segments was significantly decreased by 76.7% in group A and by 81.7% in group B compared with normal flow regions ($P<0.001$ for both groups). Segmental arterial occlusion was, therefore, followed by regional liver tis-

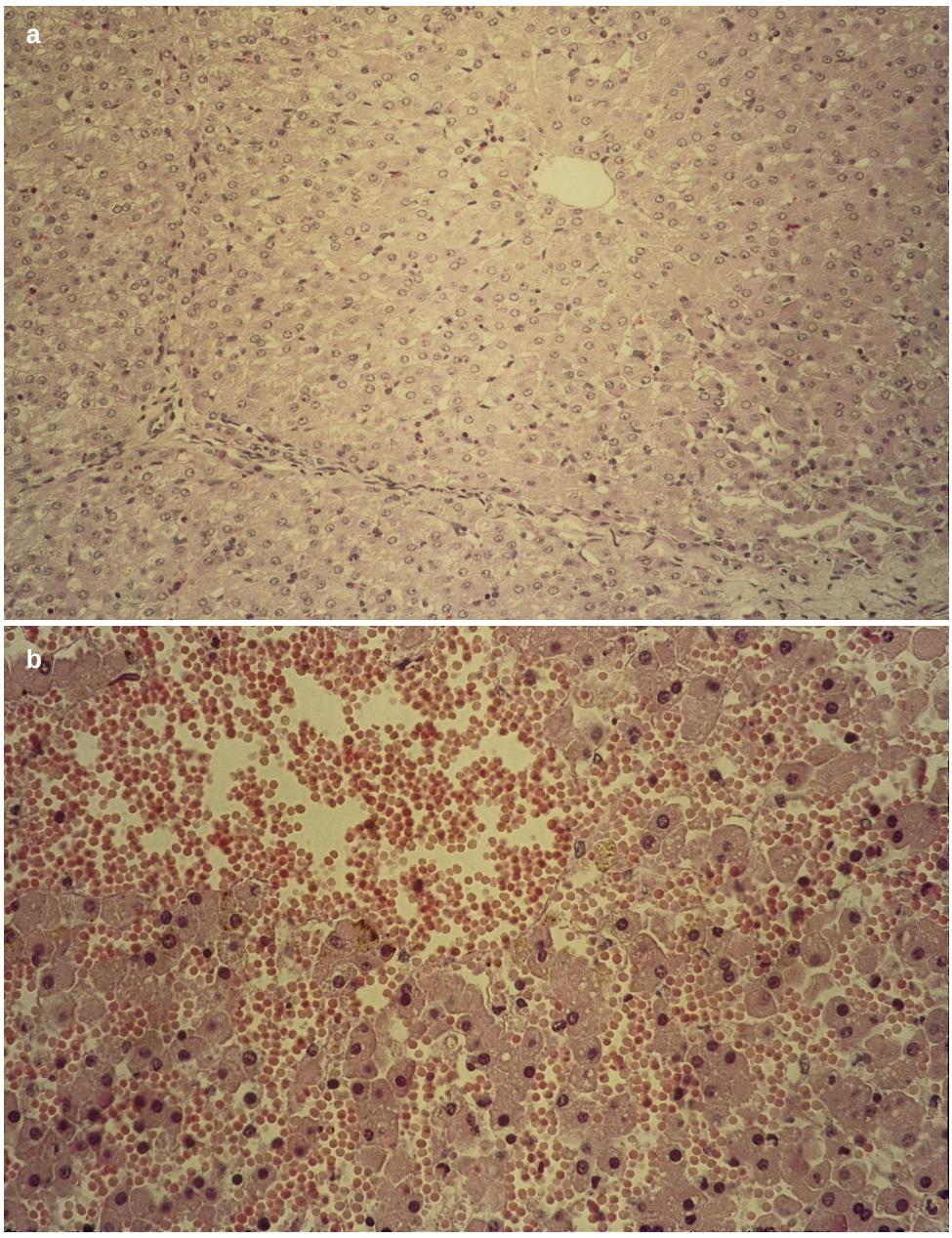

Fig. 5a, b. a Representative pictures of the haematoxylin-eosin stained section of normal pig liver (experiment no. 5, group A) with regular lobular architecture. There is a moderate diffuse Kupffer cell reaction and moderate interstitial and intracellular oedema. There is an absence of hyperaemia, bleeding and necrosis. (Original magnification ×200). **b** Haematoxylin-eosin stained section of arterially occluded liver (experiment no. 5, group A) with moderate interstitial and intracellular oedema. Severe hyperaemia is present, with ectasia of sinusoidal spaces and interstitial bleeding. There is focal liver cell necrosis. (Original magnification ×400)

sue hypoxia in both groups; high oxygen content ventilation (FiO_2=O.67, group A, n=6) did not prevent the induction of liver hypoxia. In addition, tissue sampling and PET measurements demonstrated that the [^{18}F]FMISO SUV was significantly increased in hypoxic liver. Measured by PET, the ratio of the [^{18}F]FMISO SUV between hypoxic and normal liver was 2.7 in group A and 4.4 in group B. Similar [^{18}F]FMISO SUV ratios were obtained by direct tissue sampling. Regression analysis yielded a highly significant positive correlation between the [^{18}F]FMISO SUV measured by PET and by tissue sampling (y=–0.46+1.1x; r^2=0.88; P<0.001).

Figure 6 displays the relationship between the TPO_2 results and the corresponding [^{18}F]FMISO SUV measured by PET. Clearly, a high [^{18}F]FMISO uptake was found to be associated with low TPO_2 values and vice versa. The [^{18}F]FMISO SUV was found to be closely associated with TPO_2 values under 20 mmHg, but became increasingly independent of tissue oxygenation when TPO_2 values exceeded 20 mmHg. Non-linear regression analysis yielded a squared correlation coefficient r^2 of 0.88 between the TPO_2 and [^{18}F]FMISO SUV using a mono-exponential function fit (P<0.001). In addition, regression analysis revealed significant linear correlations between the histological score and the TPO_2 (r^2=0.34, P<0.02), the [^{18}F]FMISO SUV from tissue samples (r^2=0.49, P<0.01) and [^{18}F]FMISO SUV measured by PET (r^2=0.37, P<0.01).

Table 3. Tissue-PO_2, arterial blood flow and liver tissue activities from administered [^{18}F]FMISO

Type of tissue	Group	Arterial blood flow before occlusion T_1 (microspheres) (ml min^{-1} g^{-1})	Arterial blood flow after occlusion T_3 (microspheres) (ml min^{-1} g^{-1})	[^{18}F]FMISO SUV T_4 (PET)[a]	[^{18}F]FMISO SUV T_6 (PO_2-measured tissue samples)[b]	Tissue PO_2 before PET T_3	Tissue PO_2 after PET T_5
Normal liver	A	1.24 (1.05–1.46)	1.05 (0.76–1.46)	1.4 (1.14–1.71)	1.65 (1.38–1.97)	37.6 (30.0–47.0)	26.4 (21.2–33.0)
Hypoxic liver	A	1.18 (1.05–1.32)	0.41 (0.32–0.52)*	3.84 (3.12–4.72)**	3.95 (3.49–4.46)**	6.0 (5.1–7.4)**	5.1 (4.1–6.4)**
Normal liver	B	1.35 (1.14–1.58)	1.14 (0.83–1.57)	1.31 (1.09–1.57)	1.76 (1.48–2.1)	24.7 (15.9–38.7)	18.2 (13.3–25.1)
Hypoxic liver	B	1.64 (1.41–1.91)	0.24 (0.16–0.33)**	5.7 (4.71–6.9)**	5.3 (4.49–6.26)**	4.2 (3.2–6.0)**	3.5 (2.6–4.9)**

Data represent the geometric mean and 95% confidence limits (in parentheses)
*P<0.01, **P<0.001 (significantly different versus values in normal liver)
[a] Calculated from PET images obtained 165–180 min after tracer injection
[b] Calculated in TPO_2-measured tissue samples, obtained immediately after sacrifice

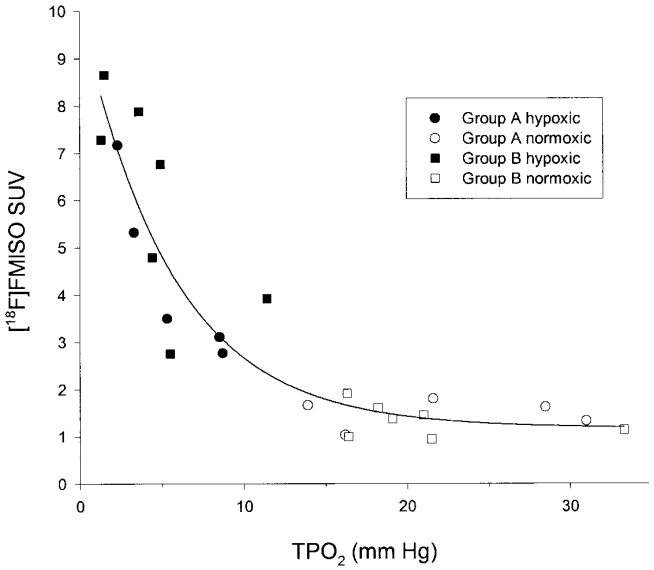

Fig. 6. Relationship between the liver tissue TPO_2 and the SUV for [^{18}F]FMISO measured by PET in hypoxic (*black*) and normoxic (*white*) liver tissue of groups A (*circles*) and B (*squares*). The exponential regression curve was obtained by non-linear fitting (y=1.19+8.9$^{(-0.78x)}$; r^2=0.88, P<0.001)

Discussion

Nitroimidazole binding to oxygen-deprived but viable cells and tissues has been extensively demonstrated [11, 16–25, 40–42]. Despite intensive investigations, the binding mechanism of nitroimidazole compounds is not yet fully understood [15]. Several studies have revealed an enhanced binding of nitroimidazoles to normal liver tissue. Enhanced misonidazole retention in adequately oxygenated liver tissue has been related to the normal metabolism of the drug [28] as well as to the fact that the liver functions at a significantly lower TPO_2 than other normally oxygenated tissues [27, 30, 31]. Previous PET studies using [^{18}F]FMISO to study tissue hypoxia suffered from the reduction of tracer delivery due to the induction of hypoxia by ischaemia (arterial occlusion). When flow decreased below 25–30% of the normal flow, [^{18}F]FMISO was retained in ischaemic brain tissue and myocardium. Enhanced [^{18}F]FMISO binding could only be found as long as the arterial blood flow remained higher than 10% of the normal flow [19, 22] because otherwise tracer delivery was critically reduced. In contrast to the particular experimental conditions of the heart and brain, due to its dual blood supply the liver is a favourable model for the study of tracer uptake under hypoxic conditions because basal tracer delivery to the hypoxic tissue is maintained after arterial occlusion by the portal circulation. However, [^{18}F]FMISO PET can only be used to estimate tissue hypoxia in vivo if the [^{18}F]FMISO uptake is defined for various tissue PO_2 values as well as for the type of tissue investigated.

In this study, we determined the spatial arterial flow distribution of the normal and arterially occluded liver using dual arterial microsphere injections and extensive multiple liver tissue sampling. The arterial blood flow before segmental arterial occlusion (T_1) was measured before any surgical manipulation at the hepatic ligament. We found a considerable intraindividual variation of the arterial blood flow in normal liver segments. The flow distribution was found to be roughly bell-shaped and skewed in the direction of high flow. Both the distribution and the range of the observed arterial hepatic blood flow values were similar to previous findings [39, 43, 44]. The arterial blood flow of normal liver segments did not differ significantly between segments. Arterial occlusion of branches of the hepatic artery decreased the

mean arterial blood flow to TPO_2-measured liver tissue significantly by 65.3% in group A and by 85.4% in group B experiments. The decrease in arterial blood flow was the result of a distinct shift of the flow distribution to the left. Interestingly, in the vast majority of flow-impaired tissue samples, the arterial blood flow was determined to be greater than zero. Arterially injected microspheres might have entered arterially occluded segments through arterio-arterial anastomoses, the existence of which has been proven previously in several species [45, 46]. In addition, arterially injected microspheres might have passed the intestinal capillary bed through arteriovenous shunts and entered the liver by the portal circulation. Previously, the amount of arteriovenous anastomotic blood flow through mesenteric organs measured by radiolabelled microspheres in dogs was found to be 3% under physiological conditions [47]. A slight increase in arteriovenous shunt flow due to the particular experimental conditions in this study (i.e. haemodilution) could explain our findings.

Before and after arterial occlusion, the distribution of the arterial blood flow was similar to the TPO_2 distribution. Both measurements displayed a clear shift of the distribution curve towards decreased values following arterial occlusion. Despite uninterrupted portal venous blood flow, segmental hepatic arterial occlusion was followed by regional liver hypoxia in both groups, as verified by PO_2 histography. Both the oxygen content of arterial and portalvenous blood and the extent of the arterial flow impairment determined the severity of tissue hypoxia. Consequently, mean TPO_2 values obtained under room air ventilation in group B were lower than in group A with oxygen-enriched ventilation. Interestingly, even a high oxygen content of the breathing air (FiO_2=0.67) and a moderate arterial flow reduction in group A did not prevent mild to moderate liver tissue hypoxia as determined by TPO_2 measurements. Haemodilution might have contributed to the enhancement of liver tissue hypoxia by decreasing the oxygen transport capacity and by consecutively reducing the portal venous blood flow due to vasoconstriction of the splanchnic circulation. Our microscopic findings further supported the results of TPO_2 measurements. The decreased oxygen supply in arterially occluded segments resulted in intracellular and interstitial oedema, which can significantly narrow the sinusoidal calibre. In addition, interstitial bleeding and sinusoidal stasis might have contributed to the development of regional liver tissue hypoxia.

To verify the existence of liver tissue hypoxia after segmental arterial occlusion and to establish the relationship between the liver TPO_2 and [^{18}F]FMISO uptake, we measured the TPO_2 directly using PO_2 histography. Mean TPO_2 values in normally perfused liver before PET measurements were 22.9 mmHg under room air and 34.0 mmHg under oxygen-enriched ventilation. While the distribution of the TPO_2 was found to be bell-shaped under room air ventilation, it shifted slightly to the right towards higher values with increasing variability under high oxygen concentration ventilation. The observed distribution changes were in good agreement with earlier findings obtained by oxygen surface electrodes under comparable ventilation conditions [48]. Arterial occlusion was followed by a distinct shift of the TPO_2 distribution curve to the left in both groups, which was associated with a significant decrease in the mean TPO_2.

Polarographic oxygen electrodes have been widely used to measure the oxygen tension in various tissues. Measurements have been taken under room air ventilation [32,33] as well as during anaesthesia [49]. In animal experiments, where the TPO_2 was measured under both anaesthesia and room air ventilation conditions, no influence of anaesthetic drugs was observed [50], but potential effects might have been masked by the high variability of TPO_2 measurements. While the effects of the commonly used anaesthetic combination of nitrous oxygen and isoflurane – as performed in this study – on the hepatic TPO_2 have not been investigated so far, influences on liver surface oxygenation have been reported. Spiegel et al. [48] found a slight decrease in hepatic surface TPO_2 caused by isoflurane inhalation. Even in the event that the liver TPO_2 measurements were influenced in any way by our particular experimental conditions, these influences, if they did indeed exist, would have affected measurements in hypoxic and normal liver tissues to the same degree and thus would have played a minor role.

Previous studies comparing the fraction of hypoxic tissue determined by autoradiography and by PO_2 histography measurements found inconsistent results. While Kavanagh et al. [50] were unable to detect a significant correlation between the mean TPO_2 and [^{3}H]misonidazole binding in different murine tumours, Casciari et al. [51] found a significant correlation between the hypoxic fraction of tumour spheroids and [^{3}H]FMISO uptake. Discrepancies between [^{3}H]misonidazole binding and TPO_2 measurements might have been related to the fact that the proportion of hypoxic cells per tissue did not necessarily correlate with the distribution of TPO_2 values measured in that tissue. (Firstly, the measurement of the hypoxic cell proportion within a tissue does not account for the severity of cell hypoxia present. Secondly, since [^{18}F]FMISO does not accumulate in necrotic tissues and tumours frequently contain necrotic regions, these discrepancies might also have been related to necrotic tissue within the tumours.)

To our knowledge, this is the first study on dual measurements with direct TPO_2 determination and [^{18}F]FMISO uptake measurements in vivo. As displayed in Fig. 6, we found a significant non-linear inverse relationship between the TPO_2 and the [^{18}F]FMISO SUV. Below TPO_2 values of 20 mmHg, the decrease in TPO_2 was associated with an increase in the [^{18}F]FMISO SUV to a maximum of approximately 10 in severely hypoxic liver tissues. Above TPO_2 values of 20 mmHg, the [^{18}F]FMISO SUV could not predict the TPO_2 with satisfying accuracy; thus the [^{18}F]FMISO SUV became increasingly independent of the TPO_2. Based on physio-

logical considerations and our experimental findings, an exponential function was applied to describe the relationship.

The kinetics of [^{18}F]FMISO tissue distribution was fundamentally different between normal and hypoxic liver. In normal liver, the tissue activities resulting from [^{18}F]FMISO administrations followed a decrease in plasma. The slightly higher [^{18}F] activities in normal liver compared with plasma were most probably related to drug metabolism within the liver parenchyma, including the biliary excretion of the drug. In hypoxic liver tissue, the activity from administered [^{18}F]FMISO accumulated over time. Under room air ventilation, the activity curve exceeded time-equivalent values of oxygen-ventilated cases. Most importantly, the ratio of the [^{18}F]FMISO SUV between hypoxic and normoxic liver tissue increased with increasing time post injection. Consequently, the identification of liver tissue accumulating [^{18}F]FMISO became increasingly clear with time. We performed prolonged image acquisitions, since the [^{18}F]FMISO clearance from blood was overly long for imaging purposes. At the end of the 3-h dynamic study, an excellent image quality was obtained. For the estimation of liver PO_2 in clinical routine, a static [^{18}F]FMISO PET scan with SUV measurements around 3 h after tracer injection would be sufficient.

Conclusion

Misonidazole binding to the liver tissue is mainly dependent on the tissue's oxygen concentration and therefore provides a model for studying regional oxygen distribution within liver tissue in vivo. In spite of the hepatic metabolism of nitroimidazoles, [^{18}F]FMISO is a promising PET tracer for liver hypoxia imaging. Under the condition of sufficient tracer delivery, [^{18}F]FMISO PET allows quantitative measurements of the liver tissue oxygenation in vivo. Clinical significance derives from the potential to quantify tissue oxygenation in a variety of liver function disorders, especially in hypoxia-associated chronic ethanol consumption, anoxia-reoxygenation injury and hypoxia-associated liver transplant dysfunctions. This method allows the assessment of responses to therapeutic interventions in serial studies and therefore might play an important role in clinical decision making in the future.

Acknowledgements. The authors thank all members of the PET facility and Radiopharmacy of the Nuclear Medicine Department of the University of Tübingen for their skilled technical assistance and tracer productions as well as their extensive support. We also thank Prof. Dr. K. Dietz for statistical and Dr. M. Wehrmann for histological evaluations, and Mrs. Wolf and Mrs. Schäfer for their excellent assistance during operations. Funding sources were DFG (Deutsche Forschungsgemeinschaft) grant No. PI 242/2-1 and the "fortune program" of the University of Tübingen

References

1. Lemasters JJ, DiGuiseppi J, Nieminen A-L, Herman B. Blebbing, free Ca^{2+} and mitochondrial membrane potential preceding cell death in hepatocytes. *Nature* 1987; 325: 78–81.
2. Luca A, Garcia-Pagan JC, Bosch J, Feu F, Caballeria J, Groszmann RJ, Rodes J. Effects of ethanol consumption on hepatic hemodynamics in patients with alcoholic cirrhosis. *Gastroenterology* 1997; 112: 1284–1289.
3. Adashi Y, Moore LE, Bradford BU, Gao W, Thurman RG. Antibiotics prevent liver injury in rats following long-term exposure to ethanol. *Gastroenterology* 1995; 108: 218–224.
4. Arteel GE, Iimuro Y, Yin M, Raleigh JA, Thurman RG. Chronic enteral ethanol treatment causes hypoxia in rat liver tissue in vivo. *Hepatology* 1997; 25: 920–926.
5. Stubbs M, Rodrigues L, Howe FA, Wang J, Jeong KS, Veech RL, Griffiths JR. Metabolic consequences of a reversed pH gradient in rat tumors. *Cancer Res* 1994; 54: 4011–4016.
6. Shaw BW, Gordon RD, Iwatsuki S, Starzl TE. Retransplantation of the liver. *Semin Liver Dis* 1985; 5: 394–401.
7. Forbes RD, Guttman RD, Gomersall M, Hibberd J. A controlled serial ultrastructural tracer study of first-set cardiac allograft rejection in the rat. *Am J Pathol* 1983; 111: 184–196.
8. Matsumoto Y, McCaughan GW, Painter DM, Bishop GA. Evidence that portal tract microvascular destruction precedes bile duct loss in human liver allograft rejection. *Transplantation* 1993; 56: 69–75.
9. Gadano A, Durand F, Degott C, Dosguet C, Moreau R, Hadengue A, Widmann JJ, Vachiery F, Elman A, Sogni P, Yang S, Valla D, Bernuau J, Belghiti J, Erlinger S, Lebrec D. Studies of portal hemodynamics and hepatic oxygen consumption during acute liver allograft rejection. *Transplantation* 1997; 27: 1188–1192.
10. Honig CR, Gayeski TEJ, Federspiel W, Clark ACP. Muscle O_2 gradients from hemoglobin to cytochrome: new concepts, new complexities. *Adv Med Biol* 1984; 169: 23–38.
11. Martin GV, Caldwell JH, Rasey JS, Grunbaum Z, Cerqueira M, Krohn KA. Enhanced binding of the hypoxic cell marker [^{3}H]fluoromisonidazole in ischemic myocardium. *J Nucl Med* 1989; 30: 194–201.
12. Knox RJ, Knight RC, Edwards DI. Studies on the action of nitroimidazole drugs. The products of nitroimidazoles in a radiolytic model system. *Int J Radiat Oncol Biol Phys* 1983; 10: 1323–1326.
13. Franko AJ. Misonidazole and other hypoxia markers: metabolism and applications. *Int J Radiat Oncol Biol Phys* 1986; 12: 1195–1202.
14. Whitmore GF, Varghese AJ. The biological properties of reduced nitroheterocyclies and possible underlying biochemical mechanisms. *Biochem Pharm* 1986; 35: 97–103.
15. Nunn A, Linder K, Strauss HW. Nitroimidazoles and imaging hypoxia. *Eur J Nucl Med* 1995; 22: 265–280.
16. Rasey JS, Koh W-J, Grierson JR, Grunbaum Z, Krohn KA. Radiolabeled fluoromisonidazole as an imaging agent for tumor hypoxia. *Int J Radiat Oncol Biol Phys* 1989; 17: 985–991.
17. Koh W-J, Bergman KS, Rasey JS, Peterson LM, Evans ML, Graham MM, Grierson JR, Lindsley KL, Lewellen TK, Krohn KA, Griffin TW. Evaluation of oxygenation status during fractionated radiotherapy in human nonsmall cell lung cancers using [F-18]fluoromisonidazole positron emission tomography. *Int J Radiat Oncol Biol Phys* 1995; 33: 391–398.
18. Chapman JD, Baer K, Lee J. Characteristics of the metabolism-induced binding of misonidazole to hypoxic mammalian cells. *Cancer Res* 1983; 43: 1523–1528.

19. Hoffmann JM, Rasey JS, Spence A, Shaw D, Krohn KA. Binding of the hypoxia tracer [^{3}H]misonidazole in cerebral ischemia. *Stroke* 1987; 18: 168–176.
20. Liu R-S, Chu L-S, Yen S-H, Chang C-P, Chou K-L, Wu L-C, Chang C-W, Lui M-T, Chen KY, Yeh S-H. Detection of anaerobic odontogenic infections by fluorine-18 fluoromisonidazole. *Eur J Nucl Med* 1996; 23: 1384–1387.
21. Martin GV, Cerqueira MD, Caldwell JH, Rasey JS, Embree I, Krohn KA. Fluoromisonidazole: a metabolic marker of myocyte hypoxia. *Circ Res* 1990; 67: 240–244.
22. Shelton ME, Dence CS, Hwang D-R, Welch MJ, Bergmann SR. Myocardial kinetics of fluorine-18 misonidazole: a marker of hypoxic myocardium. *J Nucl Med* 1989; 30: 351–358.
23. Shelton MC, Dence CS, Hwang D-R, Herrero P, Welch MJ, Bergmann SR. In vivo delineation of myocardial hypoxia during coronary occlusion using fluorine-18 fluoromisonidazole and positron emission tomography: a potential approach for identification of jeopardized myocardium. *J Am Coll Cardiol* 1990; 16: 477–485.
24. Martin GV, Biskupiak JE, Caldwell JH, Rasey JS, Krohn KA. Characterization of iodovinylmisonidazole as a marker for myocardial hypoxia. *J Nucl Med* 1993; 34: 918–924.
25. Caldwell JH, Revenaugh JR, Martin GV, Johnson PM, Rasey JS, Krohn KA. Comparison of fluorine-18-fluorodeoxyglucose and tritiated fluoromisonidazole uptake during low-flow ischemia. *J Nucl Med* 1995; 36: 1633–1638.
26. Casciari JJ, Graham MM, Rasey JS. A modeling approach for quantifiying tumor hypoxia with [F-18]fluoromisonidazole PET time-activity data. *Med Phys* 1995; 22: 1127–1139.
27. Maxwell AP, MacManus MP, Gardiner TA. Misonidazole binding in murine liver tissue: a marker for cellular hypoxia in vivo. *Gastroenterology* 1989; 97: 1300–1303.
28. McManus ME, Monks A, Collins JM, White R, Strong JM. Nonlinear pharmacokinetics of misonidazole and desmethylmisonidazole in the isolated perfused rat liver. *J Pharmacol Exp Ther* 1981; 219: 669–674.
29. Smith BR, Born JL, Garcia DJ. Influence of hypoxia on the metabolism and excretion of misonidazole by the isolated perfused rat liver – a model system. *Biochem Pharmacol* 1983; 32: 1609–1612.
30. Van Os-Corby DJ, Koch CJ, Chapman JD. Is misonidazole binding to mouse tissues a measure of cellular pO_2? *Biochem Pharmacol* 1987; 36: 3487–3494.
31. Cobb LM, Path FRC, Nolan J. Autoradiographic study of tritium-labeled misonidazole in the mouse. *Int J Radiat Oncol Biol Phys* 1989; 16: 953–956.
32. Vaupel P, Schlenger K, Knoop C, Vaupel P. Oxygenation of carcinomas of the uterine cervix: evaluation by computerized O_2 tension measurements. *Cancer Res* 1991; 51: 6098–6102.
33. Terris DJ, Dunphy EP. Oxygen tension measurements of head and neck cancers. *Arch Otolaryngol Head Neck Surg* 1994; 120: 283–287.
34. Grierson JR, Link JM, Mathis CA, Rasey JS, Krohn KA. A radiosynthesis of fluorine-18 fluoromisonidazole. *J Nucl Med* 1989; 30: 343–350.
35. Solbach M, Machulla H-J. Yield dependence of [^{18}F]FMISO on different reaction parameters. *J Lab Comp Radiopharm* 1995; 37: 199–201.
36. DeGrado TR, Turkington TG, Williams JJ, Stearns CW, Hoffman JM, Coleman RE. Performance characteristics of a whole-body PET scanner. *J Nucl Med* 1994; 35: 1398–1406.
37. Oldhafer KJ. Der Ischämie- und Reperfusionsschaden bei orthotoper Lebertransplantation. Eine tierexperimentelle Studie. In: *Beiträge zur Transplantationsmedizin*, vol 19. Pabst: Lengerich, 1994.
38. Heymann M, Payne B, Hoffman J, Rudolph A. Blood flow measurements with radionuclide-labeled particles. *Prog Cardiovasc Dis* 1977; 20: 55–79.
39. Zwissler B, Schlosser R, Weiss C, Iber V, Schwickert C, Spengler P, Messmer K. Methodological error and spatial variability of organ blood flow measurements using radiolabeled microspheres. *Res Exp Med Berl* 1991; 191: 47–63.
40. Rasey JS, Nelson NJ, Chin L, Evans ML, Grunbaum Z. Characteristics of the binding of labeled fluoromisonidazole in cells in vitro. *Radiat Res* 1990; 122: 301–308.
41. Cobb LM, Path FRC, Nolan J, Butler S. Tissue distribution of ^{14}C- and ^{3}H-labelled misonidazole in the tumor-bearing mouse. *Int J Radiat Oncol Biol Phys* 1990; 18: 347–351.
42. Parliament MB, Franko AJ, Allalunis-Turner MJ, Mielke BW, Santos CL, Wolokoff BG, Mercer JR. Anomalous patterns of nitroimidazole binding adjacent to necrosis in human glioma xenografts: possible role of decreased oxygen consumption. *Br J Cancer* 1997; 75: 311–318.
43. Lifson N, Levitt DG, Griffen WO Jr, Ellis CJ. Intrahepatic distribution of hepatic blood flow: double-input studies. *Am J Physiol* 1970; 218: 1480–1488.
44. Ziegler SI, U Haberkorn, H Byrne, C Tong, R Schosser, H Krieter, S Kaja, Richolt JA, Lammertsma AA, Price P. Measurement of liver blood flow using oxygen-15 labeled water and dynamic positron emission tomography: limitations of model description. *Eur J Nucl Med* 1996; 23: 169–177.
45. Hales MR, Allan JS, Hall EM. Injection-corrosion studies of normal and cirrhotic livers. *Am J Path* 1959; 35: 909–941.
46. Mitra SK. The terminal distribution of the hepatic artery with special reference to arterio-portal anastomosis. *J Anat* 1966; 100: 651–663.
47. Delaney JP. Arteriovenous anastomotic blood flow in the mesenteric organs. *Am J Physiol* 1969; 216: 1556–1561.
48. Spiegel H-U, Tschuschke C, Holzgreve A, Brown S, Brölsch C, Hauss J. Monitoring of liver oxygenation during neuroleptanalgesia in the dog. *J Invest Surg* 1992; 5: 315–326.
49. Rembs E, Ernst R, Bauer KH, Zumtobel V, Isselhard W. Intraoperative pO_2-measuring of liver-tissue in warm ischaemia in partial liver resection and ligature of A. hepatica dextra. In: Ehrly AM, Fleckenstein W, Landgraf H, eds. *Clinical oxygen pressure measurement. III. Tissue oxygen pressure and transcutaneous oxygen pressure.* Berlin: Blackwell, 1992.
50. Kavanagh M-C, Sun A, Hu Q, Hill RP. Comparing techniques of measuring tumor hypoxia in different murine tumors: Eppendorf pO_2 histograph, [^{3}H]nisonidazole binding and paired survival assay. *Radiat Res* 1996; 145: 491–500.
51. Casciari JJ, Rasey JS. Determination of the radiobiologically hypoxic fraction in multicellular spheroids from data on the uptake of [^{3}H]fluoromisonidazole. *Radiat Res* 1995; 141: 28–36.